Available online at www.sciencedirect.com
SCIENCE DIRECT®
Journal of Solid State Chemistry 179 (2006) 597–604
JOURNAL OF SOLID STATE CHEMISTRY
www.elsevier.com/locate/jssc

Rapid communication

Structure, energy band, and optical properties of $NaLa(PO_3)_4$ crystal

J. Zhu, W.-D. Cheng*, D.-S. Wu, H. Zhang, Y.-J. Gong, H.-N. Tong

Chinese Academy of Sciences, State Key Laboratory of Structural Chemistry, The Graduate School of the Chinese Academy of Sciences, Fujian Institute of Research on the Structure of Matter, Yang Qiao Xi Road No. 155, Fuzhou, Fujian 350002, China

Received 29 August 2005; received in revised form 24 October 2005; accepted 26 October 2005
Available online 28 November 2005

Abstract

An alkali metal-rare earth phosphate crystal of $NaLa(PO_3)_4$ has been synthesized by high temperature solid-state reactions and structurally characterized by single crystal X-ray diffraction analysis, for the first time. It crystallizes in the monoclinic $P2_1/n$ space group with lattice parameters: $a = 7.2655(3)$, $b = 13.1952(5)$, $c = 10.0760(1)$ Å, $\beta = 90.382°(1)$, $V = 965.96(5)$ Å^3, $Z = 4$. It is composed of LaO_8 polyhedra and $[(PO_3)_4]^{4-}$ chains sharing oxygen atoms to form a three-dimensional framework, delimiting intersecting tunnels in which the sodium ions are located. The IR spectrum, absorption spectrum, and emission spectrum of the compound have been investigated. The absorption edge is located at 340 nm (3.60 eV). The calculated total and partial densities of states indicate that the top of valence bands is mainly built upon O-2*p* states which interact with P-3*p* states via σ (P–O) interactions, and the low conduction bands mostly originates from unoccupied La-5*d* states. The P–O bond is mostly covalent in character, and the ionic character of the Na–O bond is larger than that in the La–O bond.

Keywords: Crystal structure; Energy band; Phosphate; Optical properties

1. Introduction

Inorganic phosphates with the general formula $M^{I}M^{III}(PO_3)_4$ (M^{I} = alkali metal, M^{III} = rare earth metal) have been extensively investigated in the past years due to their interesting optical properties [1–7]. For instance, $KNd(PO_3)_4$ crystal not only is potentially useful as laser material for miniature laser devices [1], but also allows nonlinear optical processes [2]. However, to our knowledge, the crystal structure and properties of phosphate containing lanthanum in combination with sodium is not reported in the $M^{I}M^{III}(PO_3)_4$ family. In order to find new materials with optimal properties and enrich this family of compounds, we successfully synthesized the solid-state compound $NaLa(PO_3)_4$ in our laboratory.

In this study, the synthesis by the high temperature solid-state reactions and the single-crystal structural determination are reported for the title compound, and luminescent property of the compound is studied by the absorption spectrum and the emission spectrum. Furthermore, the calculations of crystal energy band structure and optical response function have been made in order to understand the chemical bonding properties and electronic origins of optical transition for $NaLa(PO_3)_4$ crystal.

2. Experimental and computational procedures

2.1. Synthesis and analysis

Single crystals of $NaLa(PO_3)_4$ were grown by melting a mixture containing NaCl (Analytical reagent), La_2O_3 (Analytical reagent), and $NH_4H_2PO_4$ (Analytical reagent) in a molar ratio corresponding to Na/La/P = 3:1:5. The mixture was ground into fine powder in an agate mortar, transferred to a platinum crucible and preheated at a low temperature of 573 K for 4 h. Then, the sinter was reground and continuously heated at 1273 K for 24 h. The mixture was cooled to 1073 K at a rate of 2 K/h and finally

*Corresponding author. Fax: +86 591 371 4946.
E-mail address: cwd@ms.fjirsm.ac.cn (W.-D. Cheng).

0022-4596/$ - see front matter © 2005 Elsevier Inc. All rights reserved.
doi:10.1016/j.jssc.2005.10.040

air-quenched to room temperature. A few colorless crystals with needle were obtained from the melt of the mixture.

Polycrystalline samples of $NaLa(PO_3)_4$ were synthesized by solid-state reactions of stoichiometric amounts (Na/La/P = 1:1:4) of analytical reagent Na_2CO_3, La_2O_3, and $NH_4H_2PO_4$. The pulverous mixture was allowed to react at 973 K for 40 h with several intermediate grindings in an opening Pt crucible. The products were analyzed by powder XRD.

2.2. X-ray single crystal structure determination

A single crystal of $NaLa(PO_3)_4$ with approximate dimensions of $0.36 \times 0.12 \times 0.10\,mm^3$ was selected for X-ray Diffraction determination. The diffraction data were collected on a Siemens SMART CCD diffractometer with graphite-monochromated Mo$K\alpha$ radiation ($\lambda = 0.71073$ Å) using the $\omega/2\theta$ scan mode at the temperature of 273 K. An empirical absorption correction was applied using SADABS program. The structure of the title compound was solved using direct methods and refined on F^2 by full-matrix least-squares method with the SHELXL97 program package [8]. The position of the La atom was refined by the application of the direct method, and the remaining atoms were located in succeeding difference Fourier synthesis. Further details of the X-ray structural analysis are given in Table 1. The atomic coordinates and thermal parameters are listed in Table 2. Selected bond lengths and angles are given in Table 3. In order to confirm the chemical composition of the compound, the contents (weight percentages) of Na, La, and P elements were measured by the ICP method. The results obtained are in agreement with those obtained by the refinement of the crystal structure, as shown in Table 4.

2.3. Spectral measurements

The samples used for spectral measurements were polycrystalline powder synthesized by solid-state reactions. To give evidence that it contains pure phase of sample, we determined the powder XRD pattern of $NaLa(PO_3)_4$ using RIGAKU DMAX2500 diffractometer with Cu$K\alpha$ radiation (step size of 0.05° and range $2\theta = 10-80°$). The Rietveld refinement [9] was carried out with the Rietica program [10]. Fig. 1 gives the powder XRD pattern of $NaLa(PO_3)_4$ which compares with the simulated one, confirming the monophasic nature of the prepared samples. The IR spectrum was recorded in the 4000–400 cm^{-1} region by using KBr pellet on a PerKin–Elmer Spectrum One FT-IR spectrophotometer. The absorption spectrum was recorded on a cary-500 UV/VIS/NIR spectrophotometer in the wavelength range of 200–800 nm. The emission spectrum was measured on a FL/FS 900 time resolved fluorescence spectrometer using Xe lamp at room temperature.

Table 1
Crystal data and structure refinement for $NaLa(PO_3)_4$

Formula	$NaLa(PO_3)_4$
Formula weight ($g\,mol^{-1}$)	477.78
Temperature (K)	273(2)
Wavelength (Å)	0.71073
Crystal system	Monoclinic
Space group	$P2_1/n$
Unit cell dimensions	$a = 7.2655(3)$ Å
	$b = 13.1952(5)$ Å
	$c = 10.0760(1)$ Å
	$\beta = 90.382°(1)$
Volume, Z	965.96(5) $Å^3$, 4
D_{calc} ($g\,cm^{-3}$)	3.285
μ (mm^{-1})	5.195
F (0 0 0)	896
Crystal size (mm)	$0.36 \times 0.12 \times 0.10$
θ range (deg)	2.54–25.02
Limiting indices	$-8 \leqslant h \leqslant 8$; $-12 \leqslant k \leqslant 15$; $-5 \leqslant l \leqslant 11$
Reflections collected	2913
Independent reflections	1689($R_{int} = 0.0326$)
Refinement method	Full-matrix least-squares on F^2
GOF	1.009
Final R indices [$I > 2\sigma(I)$]	$R_1 = 0.0599$, w$R_2 = 0.1343$
R indices (all data)	$R_1 = 0.0627$, w$R_2 = 0.1363$
Largest diff. peak and hole ($e\,Å^{-3}$)	2.208 and −3.195

$R_1 = \sum ||F_{obs}| - |F_{calc}| / \sum |F_{obs}|$,
$wR_2 = [\sum w(F^2_{obs} - F^2_{calc})^2 / \sum w(F^2_o)]^{1/2}$.

Table 2
Atomic coordinates and equivalent isotropic displacement parameters for $NaLa(PO_3)_4$

Atom	x	y	z	U_{eq} [a]
La	0.01340(9)	0.28350(5)	0.47575(7)	0.0070(3)
P1	0.2480(4)	0.0982(2)	0.2431(3)	0.0075(7)
P2	−0.1158(4)	0.1139(2)	0.7649(3)	0.0077(7)
P3	−0.3580(4)	0.1276(2)	0.3068(3)	0.0076(7)
P4	0.2710(4)	0.0886(2)	0.6939(3)	0.0085(7)
Na	0.0001(8)	0.2207(5)	0.0684(6)	0.0222(13)
O1	0.2108(12)	−0.0154(7)	0.2885(8)	0.0127(19)
O2	0.2415(12)	0.1590(7)	0.5807(9)	0.015(2)
O3	−0.1313(12)	0.1899(7)	0.6561(9)	0.0121(19)
O4	−0.2907(11)	0.2085(7)	0.3975(8)	0.0100(18)
O5	0.0923(12)	0.0816(7)	0.7837(9)	0.014(2)
O6	0.0953(12)	0.1625(7)	0.2929(9)	0.0112(18)
O7	−0.2848(12)	0.0229(7)	0.3682(9)	0.013(2)
O8	0.1824(12)	0.3662(7)	0.6637(9)	0.0131(19)
O9	0.4262(11)	0.1219(7)	0.3313(8)	0.0098(18)
O10	0.2856(12)	0.1036(7)	0.0980(9)	0.0108(18)
O11	−0.1863(12)	0.1422(7)	0.8975(8)	0.0117(19)
O12	0.4308(12)	0.1091(8)	0.7846(9)	0.016(2)

[a] U_{eq} is defined as one-third of the trace of the orthogonalized U_{ij} tensor.

2.4. Computational procedures

The crystallographic data of the solid-state compound $NaLa(PO_3)_4$ determined by X-ray were used to calculate its electronic band structure. The calculations of electronic

Table 3
Selected bond distances (Å) and angles (°) for $NaLa(PO_3)_4$

La–O3	2.441(8)	P1–O6	1.487(9)
La–O8	2.501(9)	P1–O10	1.491(9)
La–O11^{ii}	2.522(8)	P1–O1	1.590(9)
La–O10^{iii}	2.550(8)	P1–O9	1.596(8)
La–O12^{i}	2.462(9)	P2–O11	1.483(9)
La–O6	2.513(9)	P2–O3	1.489(9)
La–O4	2.541(8)	P2–O1^{v}	1.566(10)
La–O2	2.558(9)	P2–O5	1.581(9)
Na–O11^{vii}	2.416(10)	P3–O8^{i}	1.475(9)
Na–O6	2.483(10)	P3–O4	1.486(9)
Na–O10	2.603(10)	P3–O9^{vi}	1.591(9)
Na–O2^{i}	2.463(11)	P3–O7	1.602(9)
Na–O4^{ii}	2.487(10)	P4–O2	1.485(9)
Na–O8^{i}	2.756(11)	P4–O12	1.497(9)
		P4–O5	1.590(9)
		P4–O7^{v}	1.602(9)
O6–P1–O10	116.4(5)	O4–P3–O9^{vi}	105.0(5)
O6–P1–O1	108.2(5)	O8^{i}-P3–O7	111.0(5)
O10–P1–O1	111.1(5)	O4–P3–O7	105.9(5)
O6–P1–O9	107.7(5)	O9^{vi}–P3–O7	103.0(5)
O10–P1–O9	112.6(5)	O2–P4–O12	117.6(6)
O1–P1–O9	99.4(5)	O2–P4–O5	111.1(5)
O11–P2–O3	118.0(5)	O12–P4–O5	107.2(5)
O11–P2–O1^{v}	111.4(5)	O2–P4–O7^{v}	106.5(5)
O3–P2–O1^{v}	105.9(5)	O12–P4–O7^{v}	110.7(5)
O11–P2–O5	107.2(5)	O5–P4–O7^{v}	102.8(5)
O3–P2–O5	109.7(5)	P2^{v}–O1–P1	139.4(6)
O1^{v}–P2–O5	103.6(5)	P2–O5–P4	134.4(6)
O8^{i}–P3–O4	119.6(5)	P4^{v}–O7–P3	131.5(6)
O8^{i}–P3–O9^{vi}	111.0(5)	P3^{viii}–O9–P1	136.0(6)

Symmetry codes: (i) $-0.5+x, 0.5-y, -0.5+z$; (ii) $0.5+x, 0.5-y, -0.5+z$; (iii) $-0.5+x, 0.5-y, 0.5+z$; (iv) $0.5+x, 0.5-y, 0.5+z$; (v) $-x, -y, 1-z$; (vi) $-1+x, y, z$; (vii) $x, y, -1+z$; (viii) $1+x, y, z$; (ix) $x, y, 1+z$.

Table 4
The chemical composition of $NaLa(PO_3)_4$

	Na (%)	La (%)	*P* (%)
Calculated	4.81	29.07	25.93
Experimental	4.91	28.64	25.21

band structure were carried out with density functional theory (DFT) using one of the three nonlocal gradient-corrected exchange-correlation functionals (GGA-PBE) and performed with the CASTEP code [11,12], which uses a plane wave basis set for the valence electrons and norm-conserving pseudopotential [13] for the core electrons. The number of plane waves included in the basis was determined by a cutoff energy E_c of 550 eV. Pseudoatomic calculations were performed for O-$2s^2 2p^4$, P-$3s^2 3p^3$, Na-$2s^2 2p^6 3s^1$, and La-$5d^1 6s^2$. The parameters used in the calculations and convergence criteria were set by the default values of the CASTEP code [11], e.g., reciprocal space pseudopotentials representations and eigen-energy convergence tolerance 0.6792 E–06 eV. The calculations of linear optical properties were also made in this work. The imaginary part of the dielectric function, $\varepsilon_2(\omega)$, is given by the following equation:

$$\varepsilon_2(q \to O_{\hat{u}}, \hbar\omega) = \frac{2e^2\pi}{\Omega\varepsilon_0}\sum_{k,v,c} |\langle \Psi_k^c | \hat{u}\cdot r | \Psi_k^v \rangle|^2 \delta(E_k^c - E_k^v - E), \quad (1)$$

where c and v are band indexes, Ω is the volume of the system, and $\hat{u}$ is the vector defining the polarization of the incident electric field. $\varepsilon_2(\omega)$ can be thought of as detailing the real transitions between occupied and unoccupied electronic states. Since the dielectric constant describes a causal response, the real and imaginary parts are linked by a Kramers–Kronig transform [14].

$$\varepsilon_1(\omega) - 1 = \frac{2}{\pi} P \int_0^\infty \frac{\omega' \varepsilon_2(\omega') d\omega'}{\omega'^2 - \omega^2} \text{ and}$$

$$\varepsilon_2(\omega) = -\frac{2\omega}{\pi} P \int_0^\infty \frac{\varepsilon_1(\omega') d\omega'}{\omega'^2 - \omega^2}, \quad (2)$$

where P means the principal value of the integral. This transform is used to obtain the real part of the dielectric function, $\varepsilon_1(\omega)$.

3. Results and discussions

3.1. Crystal structure

The structure of $NaLa(PO_3)_4$ crystal is characterized by a three-dimensional framework with LaO_8 polyhedra linked with $[(PO_3)_4]^{4-}$ chains by La–O–P bridges. This framework delimits intersecting tunnels in which the Na^+ ions are located, each Na^+ ion being coordinated by six oxygen atoms with the Na–O bond distances ranging from 2.416(10) to 2.756(11) Å. A view of this structure projected along *b*-axis is shown in Fig. 2. The $[(PO_3)_4]^{4-}$ wavy chain is built up from $(PO_3)_4$ groups which are formed by corner-sharing of PO_4 tetrahedra along *a*-axis, as shown in Fig. 3. In PO_4 tetrahedra, the distances P–O vary from 1.475(9) to 1.602(9) Å, and the shortest distance corresponds to the non-bridging connections of P–O, whereas the largest distance is the P–O of bridges. The O–P–O angles range from 99.4(5) to 119.6(5)°, whereas the P–O–P bridge angles of the $[(PO_3)_4]^{4-}$ wavy chain vary in the interval 131.5(6)–139.4(6)° (Table 3). These values are in conformity with those found for $NaNdP_4O_{12}$ [15]. The La^{3+} cation is surrounded by eight oxygen atoms with the La–O bond distances ranging from 2.441(8) to 2.558(9) Å (Fig. 4), which compare well with the values reported in LaP_5O_{14} [16].

3.2. Spectral properties

The IR spectrum of the compound $NaLa(PO_3)_4$ is shown in Fig. 5. To assign the IR peaks to vibrational modes, we examine the modes and frequencies observed in similar compounds [17]. The broad and intense absorption bands appearing at 1313–1226, 1180–1060, 795–682, and

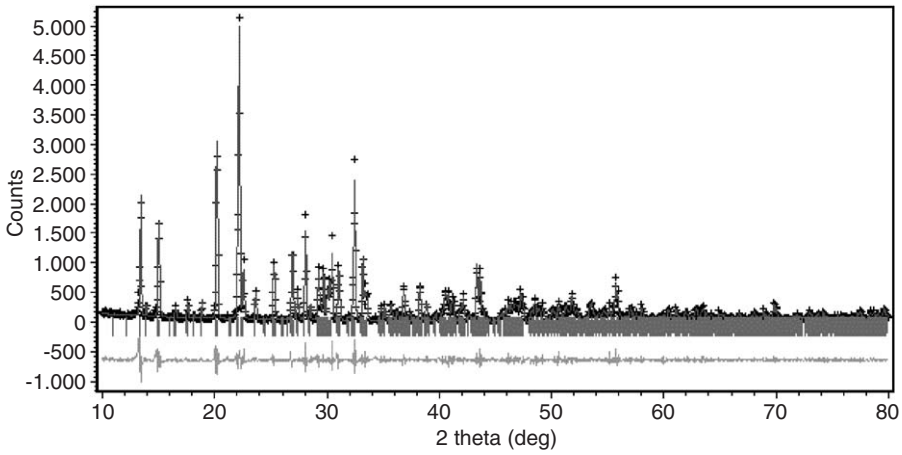

Fig. 1. Simulated and experimental powder XRD pattern for $NaLa(PO_3)_4$.

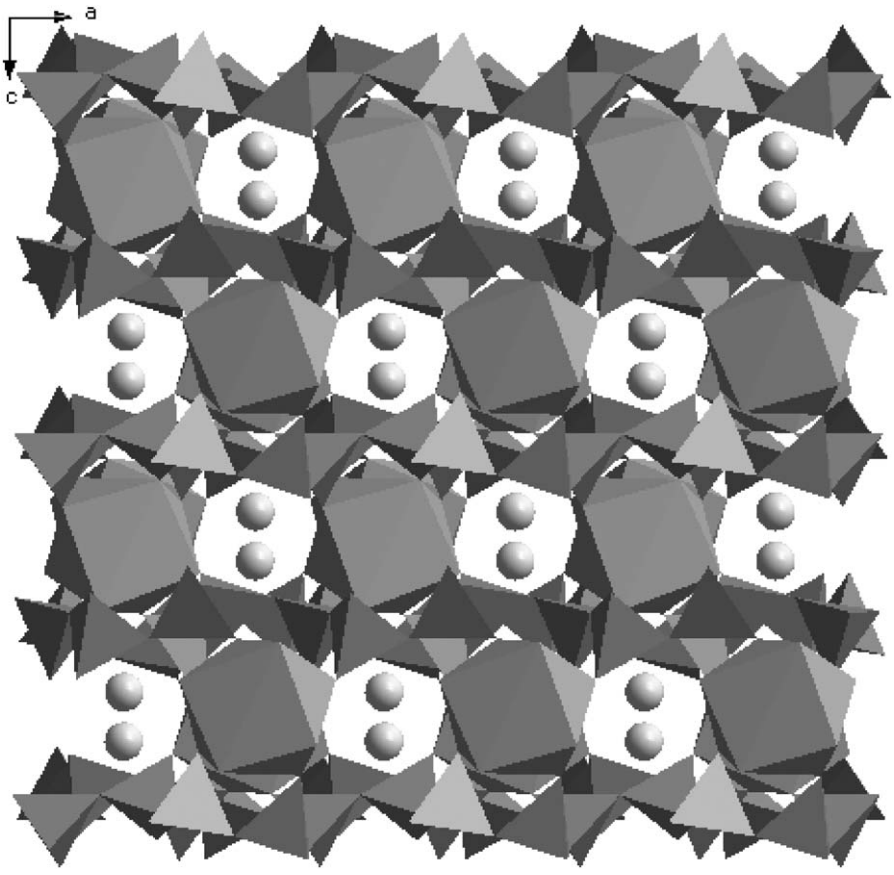

Fig. 2. Projection of the structure of $NaLa(PO_3)_4$ along *b*-axis. Solid circles: Na.

578–446 cm^{-1} can be attributed to ν_{as} (O–P–O), ν_s (O–P–O), ν_s (P–O–P), and ν_δ (P–O–P) vibrations, respectively. Also, the absorption at 913 cm^{-1} probably results from ν_{as} (P–O–P) vibrations. Fig. 6 shows the absorption spectrum of the compound. From the figure we can notice that the compound has no absorption in the range from 340 to 800 nm, and a sharp absorption peak at 237 nm as well as two shoulders at about 217 and 258 nm. The emission peaks of the compound are observed at wavelengths of 590, 612, and 698 nm from the emission spectrum under the excitation at 361 nm (Fig. 7). The luminescence located at the wavelength of 590 nm is mainly caused by the band-to-band transition, and the other two emission peaks may be assigned to relaxation from the conduction to an cationic defect site or from polaron pairs due to the large energy difference between the absorption edge and the emission peaks [18]. The two absorption shoulder peaks may be also assigned to cationic deficiency.

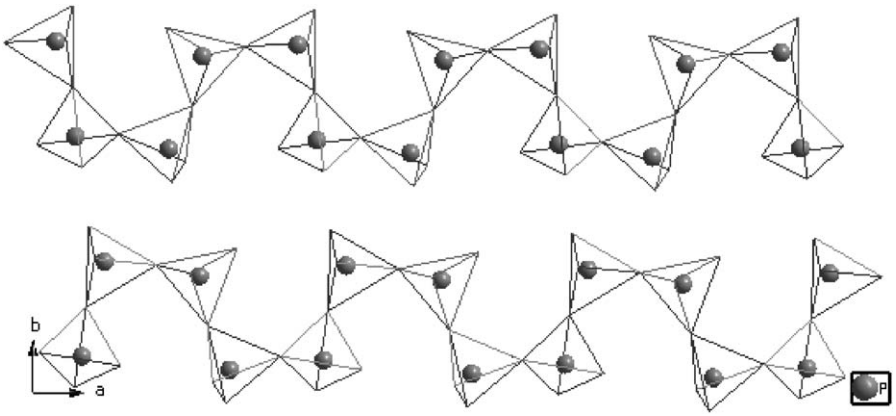

Fig. 3. The $[(PO_3)_4]^{4-}$ chains of $NaLa(PO_3)_4$ along *a*-axis.

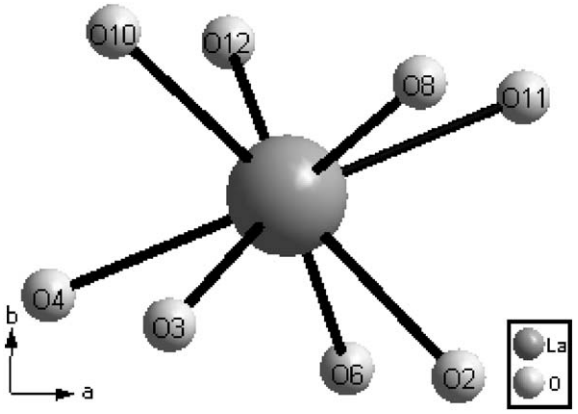

Fig. 4. The coordinated environment of the La^{3+} cation.

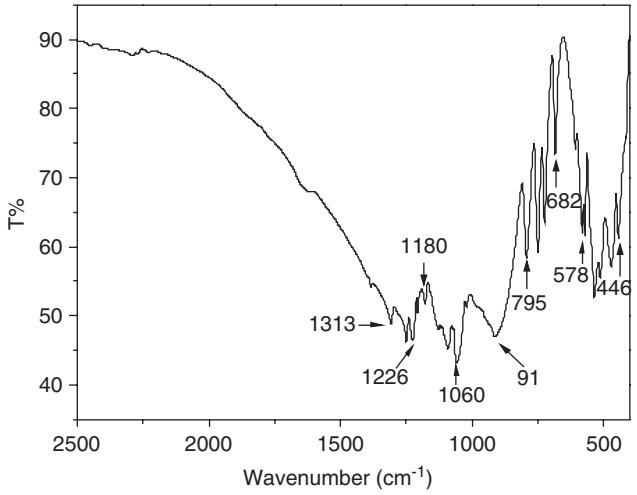

Fig. 5. The IR spectrum of $NaLa(PO_3)_4$.

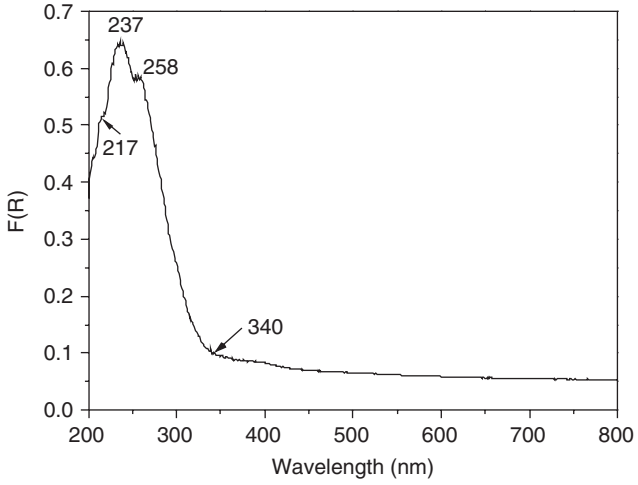

Fig. 6. The absorption spectrum of $NaLa(PO_3)_4$.

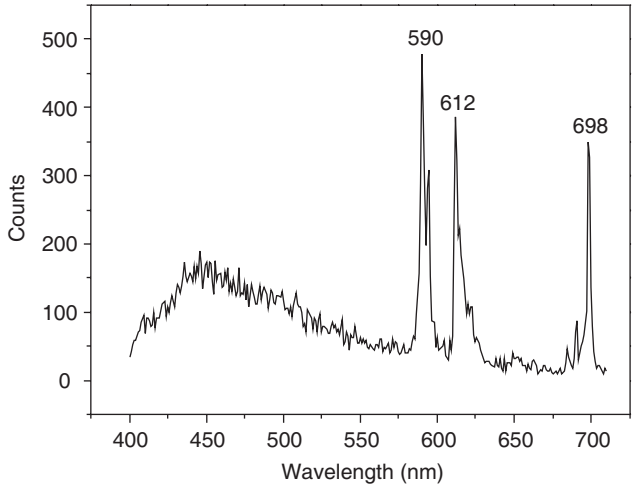

Fig. 7. The emission spectrum of $NaLa(PO_3)_4$ (excited at 361 nm).

Assignments of the electronic spectra will be also discussed in view of the band structure and density of states in the next section. Further optical studies and crystal engineering on the compound of the same series are required to gain a better understanding of these phenomena.

3.3. Band structure and density of states

The calculated band structure of $NaLa(PO_3)_4$ along high symmetry points of the first Brillouin zone is plotted in Fig. 8, where the labeled *k*-points are present as Z (0.0, 0.0, 0.5),

G (0.0, 0.0, 0.0), Y (0.0, 0.5, 0.0), A (−0.5, 0.5, 0.0), B (−0.5, 0.0, 0.0), D (−0.5, 0.0, 0.5), E (−0.5, 0.5, 0.5), and C (0.0, 0.5, 0.5). It is observed that the top of valence bands (VBs) appears to be flat and the bottom of conduction bands (CBs) have small dispersion observed along Z→G, G→Y, Y→A, and E→C. The lowest energy (4.79 eV) of conduction bands (CBs) and the highest energy (0.00 eV) of VBs are both localized at G point. According to our calculations, the solid-state compound $NaLa(PO_3)_4$ thus shows an insulator character with a direct band gap of 4.79 eV. The bands can be assigned according to total and partial densities of states (DOS), as plotted in Fig. 9. The states of Na-2*s* form the VB lying near −48.0 eV, while the sates of Na-2*p*, P-3*s*, P-3*p*, and O-2*s* create the VB ranging from −21.7 to −16.1 eV. The VB between −11.0 eV and the Fermi level (0.0 eV) are formed by the O-2*p* and P-3*p* states. The top of VBs mainly originates from O-2*p* but with small mixings of P-3*p* states via σ (P–O) interactions, and the CB between 4.79 and 7.19 eV are almost contribution from La-5*d*, P-3*s*, and P-3*p* states. Accordingly, the peak of the absorption spectrum that is observed at 237 nm (5.24 eV), as shown in Fig. 6, is assigned as the electron transitions between O-2*p* and La-5*d* states.

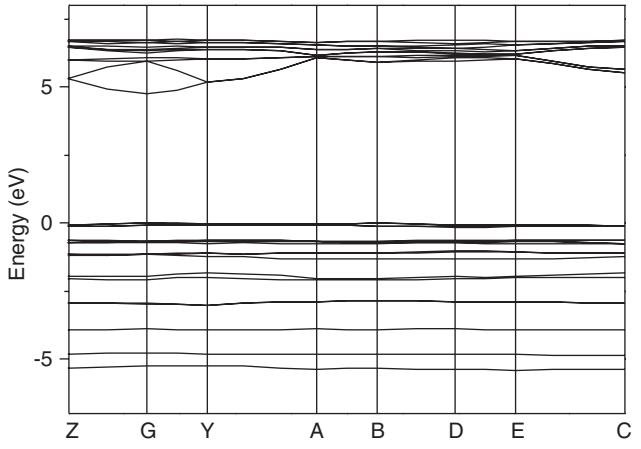

Fig. 8. The band structure of $NaLa(PO_3)_4$ (the bands below −7 eV have been cut for clarity).

Furthermore, we also elucidate the feature of chemical bonding from the nature of total and angular momentum projected DOS of $NaLa(PO_3)_4$. Comparing the total DOS with the angular momentum projected DOS displayed in Fig. 9, we observe that the densities of O-2*p* states (71 electrons/eV) is much larger than those of P-3*p* states (6.4 electrons/eV) between −6.10 and 0.0 eV. This result shows that some electrons in P-3*p* transform into the VBs and take part in the interactions between P and O atoms. This case tells us that the hybridization between P-3*p* and O-2*p* sates takes place and covalent bond character appears between P and O atoms. It is also found that the PDOS of Na-3*s* state is mainly located in conduction band and there is only weak contributions to the valence band, which determine that the Na–O bond is ionic. The chemical bonding properties are also evident from the population analysis. The calculated bond orders of the P–O, La–O, and Na–O bonds are from 0.45 to 0.81 e, 0.20 to 0.29 e, and 0.02 to 0.05 e in a unit cell of $NaLa(PO_3)_4$ (covalent single bond order is generally 1.0 e), respectively. Accordingly, we can also say that the covalent character of the P–O bond is larger than that of the La–O bond, and the ionic character of the Na–O bond is larger than that of the La–O bond in $NaLa(PO_3)_4$.

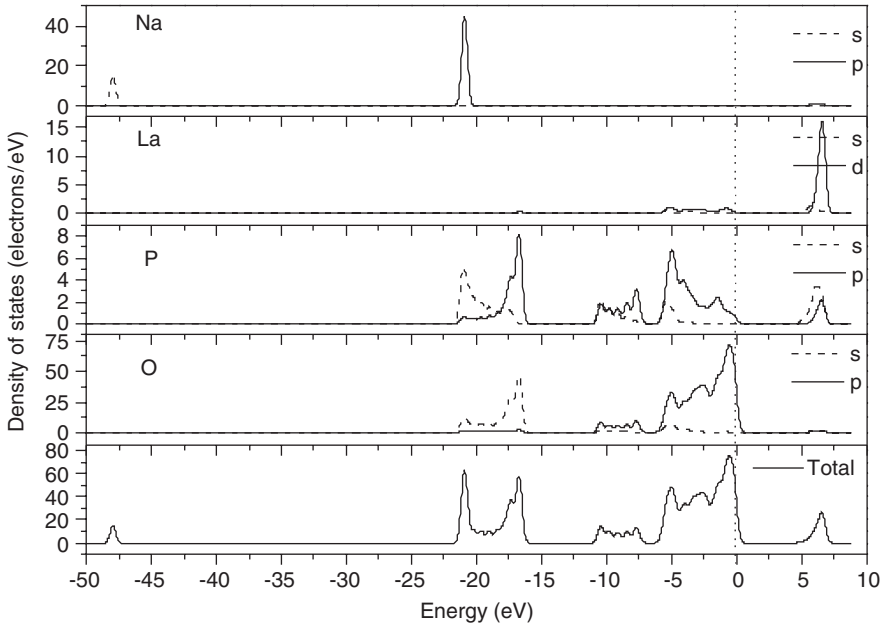

Fig. 9. The total and partial DOS of $NaLa(PO_3)_4$.

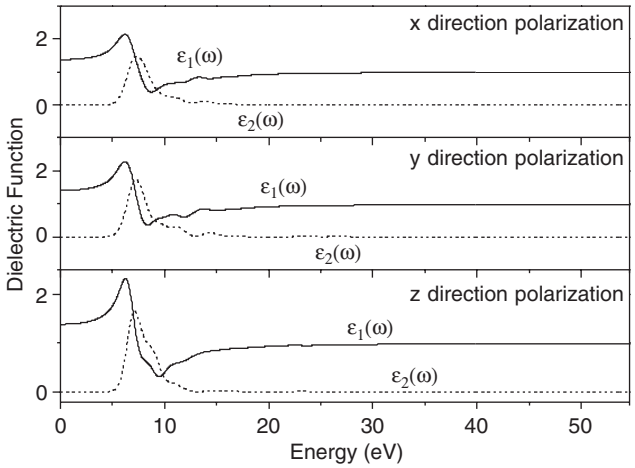

Fig. 10. The calculated dielectric function in different polarization direction of $NaLa(PO_3)_4$.

3.4. Optical properties

In order to examine the linear optical response properties of $NaLa(PO_3)_4$ crystal, we calculated the imaginary part $\varepsilon_2(\omega)$ and the real part $\varepsilon_1(\omega)$ of the frequency-dependent dielectric function without the DFT scissor-operator approximation, as displayed in Fig. 10. The part $\varepsilon_2(\omega)$ can be used to describe the real transitions between the occupied and unoccupied electronic states. It is found from the dispersion of the calculated $\varepsilon_2(\omega)$ spectra that there are absorption peaks localized at about 7.39 eV (168 nm), 7.28 eV (171 nm), and 7.16 eV (173 nm) in x, y, and z polarization directions, individually. The crystal is transparent while the wavelength is larger than 276 nm or photon energy is less than 4.50 eV. The observed ultraviolet edge of cut-off is at about 340 nm for polycrystalline power sample as shown in Fig. 6. Comparing the calculated transparent ultraviolet edge of the crystal with the observed one of power sample, we find that the transparent width of ultraviolet region is larger for the crystal than the power. It is indicated that the calculated result is reasonable. The calculated dielectric constants of static case $\varepsilon(0)$ are about 1.3671, 1.4063, and 1.3822 in x, y, and z directions, respectively. The dispersion curves of refractive index are also calculated by the relation of $n^2(\omega) = \varepsilon(\omega)$, and the refractive indexes of n_x, n_y, and n_z are 1.1750, 1.1922, and 1.1817, respectively, at a wavelength of 880 nm. The refractive index of $NaLa(PO_3)_4$ crystal has not been measured and reported, and therefore, our calculated results only compare with the observed results of the other phosphate crystals. It is reported that the observed refractive index of phosphate is generally ranging from 1.40 to 1.60 [19]. Comparing with the observed refractive index of the other phosphate crystals, our calculated refractive index of the phosphate crystal $NaLa(PO_3)_4$ may be underestimated about 15–25% at static case.

4. Conclusions

In the present work, the single-crystal structure of the compound $NaLa(PO_3)_4$ synthesized by high temperature solid-state reactions has been determined and it crystallizes in monoclinic system with space group $P2_1/n$. It is observed that the sharp absorption peak is at about 237 nm, which mainly originates from O-2p to La-5d states. The calculated band structures show that the solid-state compound of $NaLa(PO_3)_4$ is an insulator with a direct band gap of 4.79 eV. The calculated total and partial densities of states indicate that the top of valence bands is mainly built upon O-2p states which interact with P-3p states via σ (P–O) interactions, and the low of conduction bands mostly originates from unoccupied La-5d states. The calculated populations show that the interactions between P and O atoms are mainly covalent in character and those between Na and O atoms are significantly ionic, the ionic character of the Na–O bond being larger than in the La–O bond. The dispersion of the dielectric function has been calculated for $NaLa(PO_3)_4$ crystal, and it is shown that the crystal is ultraviolet transparent while the wavelength is larger than 276 nm or the photon energy is less than 4.50 eV.

5. Supporting information available

Further details on the crystal structure investigations can be obtained from the Fachinformationszentrum Karlsruhe, 76344 Eggenstein-Leopoldshafen, Germany, (fax: (49) 7247-808-666; e-mail: crysdata@fiz.Karlsruhe.de) on quoting the depository number CSD-415682).

Acknowledgment

This investigation was based on work supported by the National Natural Science Foundation of China under projects 20373073 and 90201015, the Science Foundation of the Fujian Province (No.E0210028), and the Foundation of State Key Laboratory of Structural Chemistry (No. 030060). We thank Prof. Liping Li for the fruitful discussion concerning the powder XRD pattern.

References

[1] H.Y.-P. Hong, Mat. Res. Bull. 10 (1975) 1105–1110.
[2] I. Parreu, R. Solé, Jna. Gavaldà, J. Massons, F. Díaz, M. Aguiló, Chem. Mater. 15 (2003) 5059–5064.
[3] H. Ettis, H. Naïli, T. Mhiri, Cryst. Growth Des. 3 (2003) 599–602.
[4] K. Horchani, J.C. Gâcon, M. Ferid, M. Trabelsi-Ayedi, O. Krachni, G.K. Liu, Opt. Mater. 24 (2003) 169–174.
[5] K. Horchani, J.C. Gâcon, C. Dujardin, N. Garnier, C. Garapon, M. Ferid, M. Trabelsi-Ayedi, J. Lumin. 94-95 (2001) 69–72.
[6] I. Parreu, R. Solé, Jna. Gavaldà, J. Massons, F. Díaz, M. Aguiló, Chem. Mater. 17 (2005) 822–828.
[7] M. Saito, T. Honma, Y. Benino, T. Fujiwara, T. Komatsu, Solid State Sci 6 (2004) 1013–1018.
[8] G.M. Sheldrick, SHELXTL-97 Program for Refining Crystal Structure, University of Göttingen, Göttingen, Germany, 1997.

[9] (a) H.M. Rietveld, Acta Crystallogr 22 (1967) 151;
(b) H.M. Rietveld, Acta Crystallogr 25 (1969) 589.
[10] B. A. Hunter, Lhpm-rietica, www.rietica.Org.
[11] M. Segall, P. Linda, M. Probert, C. Pickard, P. Hasnip, S. Clark, M. Payne, Materials Studio CASTEP version 2. 2, 2002.
[12] M. Segall, P. Linda, M. Probert, C. Pickard, P. Hasnip, S. Clark, M. Payne, J. Phys.: Condens. Mater. 14 (2002) 2717–2744.
[13] D.R. Hamann, M. Schluter, C. Chiang, Phys. Rev. Lett. 43 (1979) 1494–1497.
[14] J.R. Macdonald, M.K. Brachman, Rev. Mod. Phys. 28 (1956) 383.
[15] H. Koizumi, Acta Cryst. B. 32 (1976) 2254–2256.
[16] J.M. Cole, M.R. Less, J.A.K. Howard, R.J. Newport, G.A. Saunders, E. Schönherr, J. Solid State Chem. 150 (2000) 377–382.
[17] A. Jouini, M. Férid, M. Trabelsi-Ayadi, Thermochim. Acta. 400 (2003) 199–204.
[18] Y. Kawabe, A. Yamanaka, E. Hanamura, T. Kimura, Y. Takiguchi, H. Kan, Y. Tokura, J. Appl. Phys. 88 (2000) 1175–1177.
[19] J.A. Dean (Ed.), Lange's Handbook of Chemistry, Thirteenth ed, McGraw-Hill Book Company, 1985.